

# Search for Glueballs from Three-body Annihilation of $\bar{p}p$ in-Flight

Bing-Song Zou<sup>a\*</sup>

<sup>a</sup>Queen Mary and Westfield College, London E1 4NS, UK

Lattice QCD and other theoretical models predict that the  $0^{-+}$ ,  $2^{++}$  and  $2^{-+}$  glueballs have masses in the range of 2.0 to 2.4 GeV. For resonances in such an energy range, three-body decay modes are expected to be large. The strategy for looking for these glueballs and the newest results from studying Crystal Barrel data on the three-body annihilation of  $\bar{p}p$  in flight are presented.

## 1. STRATEGY FOR GLUEBALL HUNTING IN $p\bar{p}$ ANNIHILATION

Proton-antiproton annihilation is regarded as a favorable process for glueball production. For  $p\bar{p}$  annihilation, there are two possible ways to produce glueballs as shown in Fig.1(a&b), which are so called “production” and “formation” mechanisms, respectively.

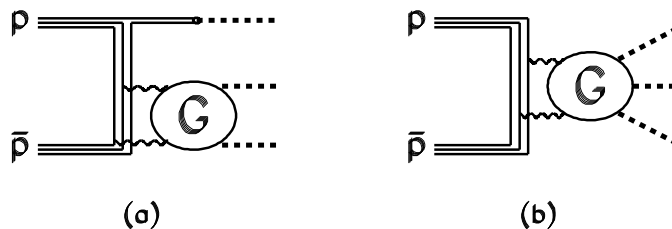


Figure 1. Glueball production mechanisms for  $p\bar{p}$  annihilation: (a) “production” mechanism; (b) “formation” mechanism. Dashed and helix lines are for mesons and gluons, respectively.

For the  $0^{++}$  glueball ground state, lattice QCD predicts its mass to be  $1.45 \sim 1.8 \text{ GeV}/c^2$  [1]. For a glueball in such a mass range to be produced from  $p\bar{p}$  annihilation, it can only come from the “production” mechanism. Indeed, by studying  $p\bar{p} \rightarrow 3\pi^0$  &  $\pi^0\eta\eta$ , Crystal Barrel Collaboration[2] discovered the  $f_0(1500)$  resonance which is now regarded as the best  $0^{++}$  glueball candidate[3]. There is also some new evidence for  $f_0(1770)$ [4].

If the  $f_0(1500)$  is really a glueball, it sets a mass scale for glueballs of other quantum numbers. The  $0^{-+}$ ,  $2^{++}$  and  $2^{-+}$  glueballs are predicted to be around  $2.1 \sim 2.4 \text{ GeV}$  by

\*Now at Institute of High Energy Physics, P.O.Box 918(4), Beijing 100039, China

various theoretical models[1,5,6]. For resonances in such an energy range, they should be mainly produced from the “formation” mechanism and three-body decay modes are expected to be large.

Crystal Barrel has taken a lot of data for all neutral final states in flight. Then the question is which three body channels we should study first. Here we can take some lessons from charmonium decays. For  $\eta_c(0^{-+})$ ,  $\chi_{c0}(0^{++})$ ,  $\chi_{c2}(2^{++})$  hadronic decays and  $J/\Psi$  radiative decays, they definitively go through two-gluon intermediate states. The  $\eta$ ,  $\eta'$ ,  $\sigma$  and  $f_0(1500)$  seem to be favoured decay products of two-gluon states[7,8]. The  $\eta\sigma$ ,  $\eta'\sigma$  and  $\eta f_0(1500)$  are expected to be large decay modes of  $0^{-+}$  glueballs while the  $\eta f_2$  and  $\eta' f_2$  are expected to be large for  $2^{-+}$  and  $2^{++}$  glueball decays. These decay modes have  $\pi^0\pi^0\eta$ ,  $\pi^0\pi^0\eta'$  and  $3\eta$  as their final states.

Hence our strategy for hunting  $0^{-+}$ ,  $2^{++}$  and  $2^{-+}$  glueballs is to study resonances formed by  $p\bar{p}$  and decaying into  $\pi^0\pi^0\eta$ ,  $\pi^0\pi^0\eta'$  and  $3\eta$  final states first.

## 2. STATUS OF THREE-BODY ANNIHILATION IN-FLIGHT

Crystal Barrel at LEAR has collected data triggering on neutral final states at beam momenta 0.6, 0.9, 1.05, 1.2, 1.35, 1.525, 1.642, 1.8 and 1.94 GeV/c, which correspond to center-of-mass energies ranging from 1.96 to 2.41 GeV/c<sup>2</sup>. An average of 8.5 million all neutral events were taken at each momentum.

These data have been processed. Rough number of selected events at each beam momentum and background level for reconstructed three-body channels from  $6\gamma$  and  $7\gamma$  events are listed in Table 1. Among them, the background level for the  $\pi^0\pi^0\omega$  channel has not been investigated yet; the background level for  $\pi^0\pi^0\eta'$  is too high to do partial wave analysis. So we have been analyzing the first four channels.

Table 1

Rough number of selected events at each beam momentum and background level for reconstructed three-body channels from  $6\gamma$  and  $7\gamma$  events.

channel	Number of Events	background level
$\pi^0\pi^0\pi^0$	$\sim 150K$	1%
$\pi^0\pi^0\eta$	$\sim 70K$	3%
$\pi^0\eta\eta$	$\sim 6K$	6%
$\eta\eta\eta$	$\sim 150$	3%
$\pi^0\pi^0\eta'$	$\sim 1K$	50%
$\pi^0\pi^0\omega$	$\sim 70K$	

For  $\pi^0\pi^0\pi^0$  channel, the most obvious contributions come from  $f_2(1270)\eta$  and  $f_0(1500)\eta$  intermediate states. The partial wave analysis is in progress.

For  $\pi^0\eta\eta$  channel, the statistics is not enough for a full partial analysis including both production and formation amplitudes. Some effective formalism was used to concentrate on searching for resonances in the production mechanism[4]. The main results are:

$f_0(1500) \rightarrow \eta\eta$  is clearly seen;  $f_0(1750 \sim 1800)$ ,  $f_0(2100)$  and  $a_2(1660)$  are confirmed; in addition there is a broad  $f_2(1980) \rightarrow \eta\eta$  with mass  $M = 1980 \pm 50$  MeV and width  $\Gamma = 500 \pm 100$  MeV.

For  $\eta\eta\eta$  channel, the statistics is low. But we can still learn something. In Fig.2, we show the real data and some Monte Carlo Dalitz plots for  $\bar{p}p \rightarrow \eta\eta\eta$  at 1.8 GeV/c.

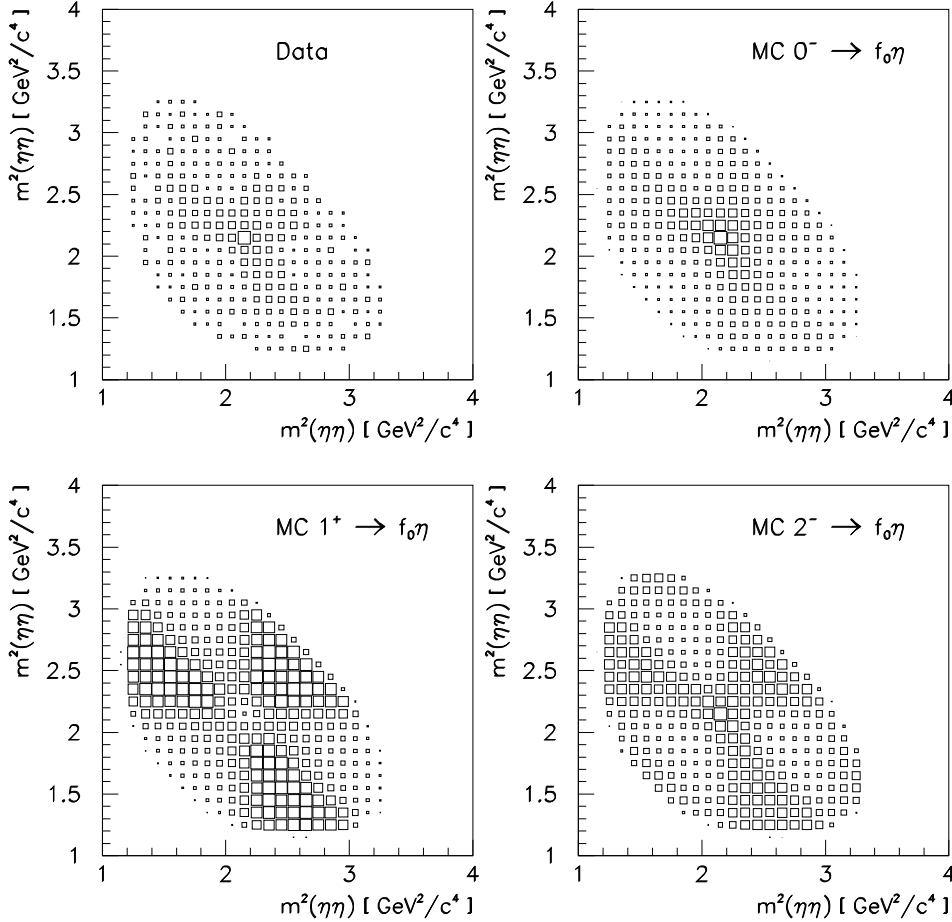


Figure 2. Real data and Monte Carlo Dalitz plots for  $\bar{p}p \rightarrow \eta\eta\eta$  at 1.8 GeV/c.

From the real data Dalitz plot in Fig.2, the  $f_0(1500)$  is obviously there. For the beam momentum of 1.8 GeV/c, the orbital angular momentum between  $f_0(1500)$  and  $\eta$  is expected to be  $\leq 2$ , which corresponds to the initial states of  $0^-(l_f = 0)$ ,  $1^+(l_f = 1)$  and  $2^-(l_f = 2)$ . From their Monte Carlo Dalitz plots in Fig.2, without fitting data, it is already clear that the  $0^- \rightarrow f_0(1500)\eta$  is the most obvious contribution to  $\bar{p}p \rightarrow \eta\eta\eta$ .

Preliminary results of the cross section for  $\bar{p}p \rightarrow \eta\eta\eta$  is shown in Fig.3. There are two peaks at about 2.15 GeV and 2.33 GeV. They may be due to statistical fluctuations. But if they are due to two resonances, they are most likely  $0^{-+}$  resonances with the  $f_0(1500)\eta$

decay mode.

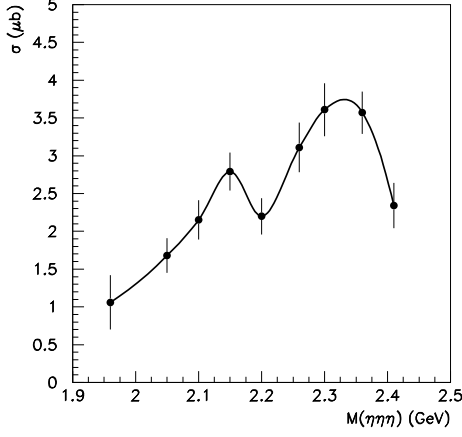


Figure 3. preliminary results of cross section for  $\bar{p}p \rightarrow \eta\eta\eta$ .

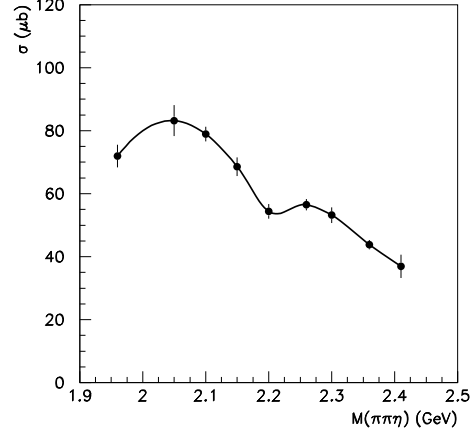


Figure 4. Cross section for  $\bar{p}p \rightarrow \pi^0\pi^0\eta$  with  $\eta \rightarrow \gamma\gamma$ .

The only channel which is favourable for hunting  $0^{-+}$ ,  $2^{++}$  and  $2^{-+}$  glueballs and has enough statistics for a full amplitude partial wave analysis is the  $\pi^0\pi^0\eta$  channel. Its cross section is shown in Fig.4. There are clear enhancements at around 2.05 and 2.3 GeV. Note that for a constant amplitude the cross section should decrease steadily as the energy increases.

For the  $\pi^0\pi^0\eta$  channel, projections on to  $M(\pi\pi)$  and  $M(\pi\eta)$  at 900, 1200, 1525 and 1800 MeV/c are shown in Fig.5. The  $f_2(1270)$ ,  $a_0(980)$  and  $a_2(1320)$  are clearly visible. The  $f_0(980)$  and  $f_0(1500)$  are visible on the  $M(\pi\pi)$  projection, but rather weak. As beam momentum increases, the  $f_2(1270)$  peak becomes stronger while the  $a_2(1320)$  peak gets weaker; this is a natural reflection of the rapidly opening phase space for  $f_2(1270)\eta$ , whose threshold is at a mass of 1820 MeV.

Based on these data, a full amplitude analysis describing both production and decay of these resonances is carried out for each momentum[9].

### 3. AMPLITUDE ANALYSIS OF $\bar{p}p \rightarrow \pi^0\pi^0\eta$

For the  $\pi^0\pi^0\eta$  final state, possible  $\bar{p}p$  initial states are  $0^{-+}$ ,  $2^{-+}$ ,  $4^{-+}$  etc. for  $\bar{p}p$  spin singlet states, and  $1^{++}$ ,  $2^{++}$ ,  $3^{++}$ ,  $4^{++}$ ,  $5^{++}$  etc. for  $\bar{p}p$  spin triplet states. For our case with center-of-mass energies below 2.41 GeV, only  $0^{-+}$ ,  $2^{-+}$ ,  $1^{++}$ ,  $2^{++}$ ,  $3^{++}$  and  $4^{++}$  are expected to be significant [10] and this has been confirmed in our analysis;  $4^{-+}$  has been tried, but is not significant. Their corresponding  $\bar{p}p$  total angular momentum J, orbital angular momentum L and total spin angular momentum S in the usual contracted form  $^{2S+1}L_J$  are:  $^1S_0$  for  $0^{-+}$ ,  $^1D_2$  for  $2^{-+}$ ,  $^3P_1$  for  $1^{++}$ ,  $^3P_2$  or  $^3F_2$  for  $2^{++}$ ,  $^3F_3$  for  $3^{++}$ , and  $^3F_4$  or  $^3H_4$  for  $4^{++}$ .

Let us choose the reaction rest frame with the z axis along the  $\bar{p}$  beam direction. Then

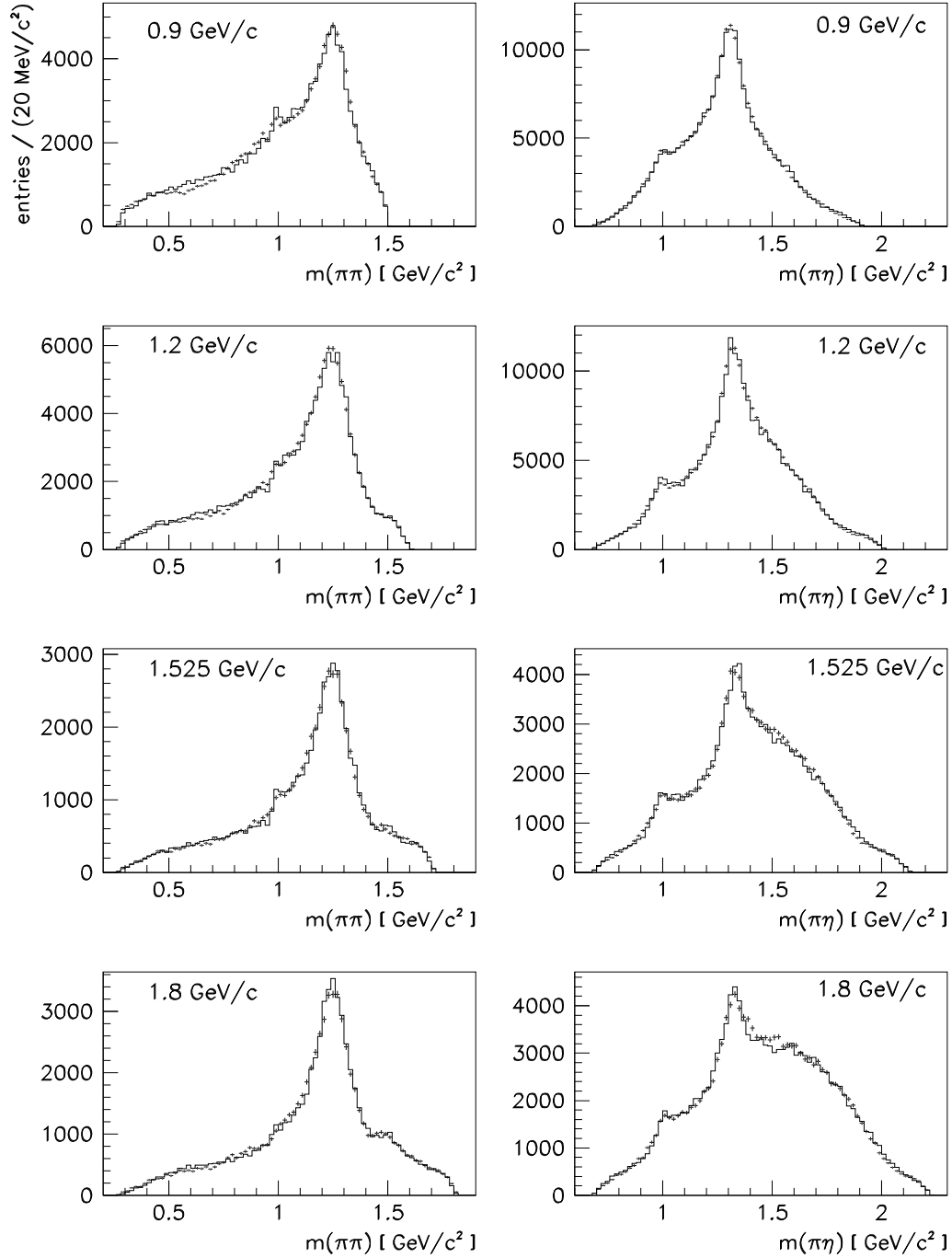


Figure 5. Data (points with error bars) and fit (solid line) of invariant mass spectra for  $\pi^0\pi^0$  (1 entry/event) and  $\pi^0\eta$  (2 entries/event). Beam momenta are given in each panel.

the squared modulus of the total transition amplitude is the following[11]:

$$\begin{aligned}
I = & |A_{0^{--}} + A_{2^{--}}|^2 + |A_{1^{++}}^{M=1} + A_{3^{++}}^{M=1}|^2 + |A_{1^{++}}^{M=-1} + A_{3^{++}}^{M=-1}|^2 \\
& + |A_{2^{++}}^{M=0} + A_{4^{++}}^{M=0}|^2 + |A_{2^{++}}^{M=1} + A_{4^{++}}^{M=1}|^2 + |A_{2^{++}}^{M=-1} + A_{4^{++}}^{M=-1}|^2 \\
& + 2Re[(A_{2^{++}}^{M=1} + A_{4^{++}}^{M=1})(A_{1^{++}}^{M=1} + A_{3^{++}}^{M=1})^* - (A_{2^{++}}^{M=-1} + A_{4^{++}}^{M=-1})(A_{1^{++}}^{M=-1} + A_{3^{++}}^{M=-1})^*]
\end{aligned} \tag{1}$$

where M is the spin projection on the z-axis. Partial wave amplitudes  $A_{JPC}$  are constructed from relativistic Lorentz covariant tensors, Breit-Wigner functions and Blatt-Weisskopf barrier factors [12,13]. The barrier factors use a radius of 1 fm. The  $f_2(1270)\eta$ ,  $a_2(1320)\pi$ ,  $a_0(980)\pi$ ,  $\sigma\eta$ ,  $f_0(980)\eta$  and  $f_0(1500)\eta$  intermediate states are considered. The  $f_0(980)$  is fitted with a Flatté formula using parameters determined previously [14]. The  $\sigma$  is fitted with the parameterization A of Ref. [14]. Other resonances are fitted with simple Breit-Wigner amplitudes using constant widths. Full formulae and additional details will be given in Ref.[9]. Based on these formulae, the data at each momentum are fitted by the maximum likelihood method.

The fit is shown in Fig.5 for the mass spectra for beam momenta at 900, 1200, 1525 and 1800 MeV/c. The quality of the fit for other beam momenta is similar. The fit to projections is obviously not perfect. These may be due to additional components such as  $a_0(1450)\pi$ ,  $a_2(1660)\pi$  and even  $\hat{\rho}(1405)\pi$  intermediate states. An angular momentum decomposition of this small effect is not possible, but fits including such states produce little effect on the dominant components. Since we are mainly interested in scanning the larger components from  $f_2(1270)\eta$ ,  $\sigma\eta$ ,  $a_2\pi$  and  $a_0(980)\pi$  intermediate states, we ignore those smaller contributions for the present study.

The data points with error bars shown in Fig.6 are our fitted results for the partial wave cross sections at each momentum for  $\bar{p}p \rightarrow \pi^0\pi^0\eta$  with  $\eta \rightarrow \gamma\gamma$ . Only those partial waves with significant contributions are presented. There are rich peak and dip structures.

For  $4^{++}$ , a peak around 2100 MeV is clear for all  $4^{++}$  partial waves. It is fitted by a Breit-Wigner amplitude with the mass and width fixed to the PDG values for the well established  $4^+$  resonance  $f_4(2050)$  [7]. The shift of the peak position is due to the centrifugal barrier factors for both initial and final states. It appears in  $f_2\eta$  and  $a_2\pi$  with comparable strength. In addition to the  $f_4(2050)$ , there is clearly another  $4^{++}$  peak around 2320 MeV in  $4^+ \rightarrow f_2\eta$  in the M=1 partial wave. This may be identified with the  $f_4(2300)$  listed in the Particle Data Tables [7].

A  $4^{++}$  resonance around this mass has also been observed by VES in  $\eta\pi^+\pi^-$  in the  $\pi A$  reaction [15].

For  $2^{++}$ , two peaks around 2020 MeV and 2350 MeV have masses and widths compatible with  $f_2(2010)$  and  $f_2(2340)$  listed by the PDG [7] as established particles. In addition, a peak around 2230 MeV shows up clearly in the  $f_2\eta$  mode. It has a mass compatible with  $\xi(2230)$  observed in  $J/\Psi$  radiative decays [7,16], but has a larger width of  $\sim 150$  MeV.

For  $2^{-+}$  and  $3^{++}$ , both have two peaks around 2050 and 2300 MeV. No corresponding entries exist for them as yet in the Particle Data Tables [7]. For  $1^{++}$ , there is a strong enhancement at the low energy end, decaying dominantly into  $a_2\pi$ .

For  $0^{-+}$ , there seems to be a broad component plus a peak in  $\eta\sigma$  at  $\sim 2140$  MeV with width  $\sim 150$  MeV. The broad component may correspond to the broad  $0^{-+}$  object used in describing  $J/\Psi$  radiative decays to  $\rho\rho$ ,  $\omega\omega$ ,  $K^*\bar{K}^*$ ,  $\phi\phi$  and  $\eta\pi\pi$  [17]. The peak at 2140 MeV decays dominantly into  $\sigma\eta$ .

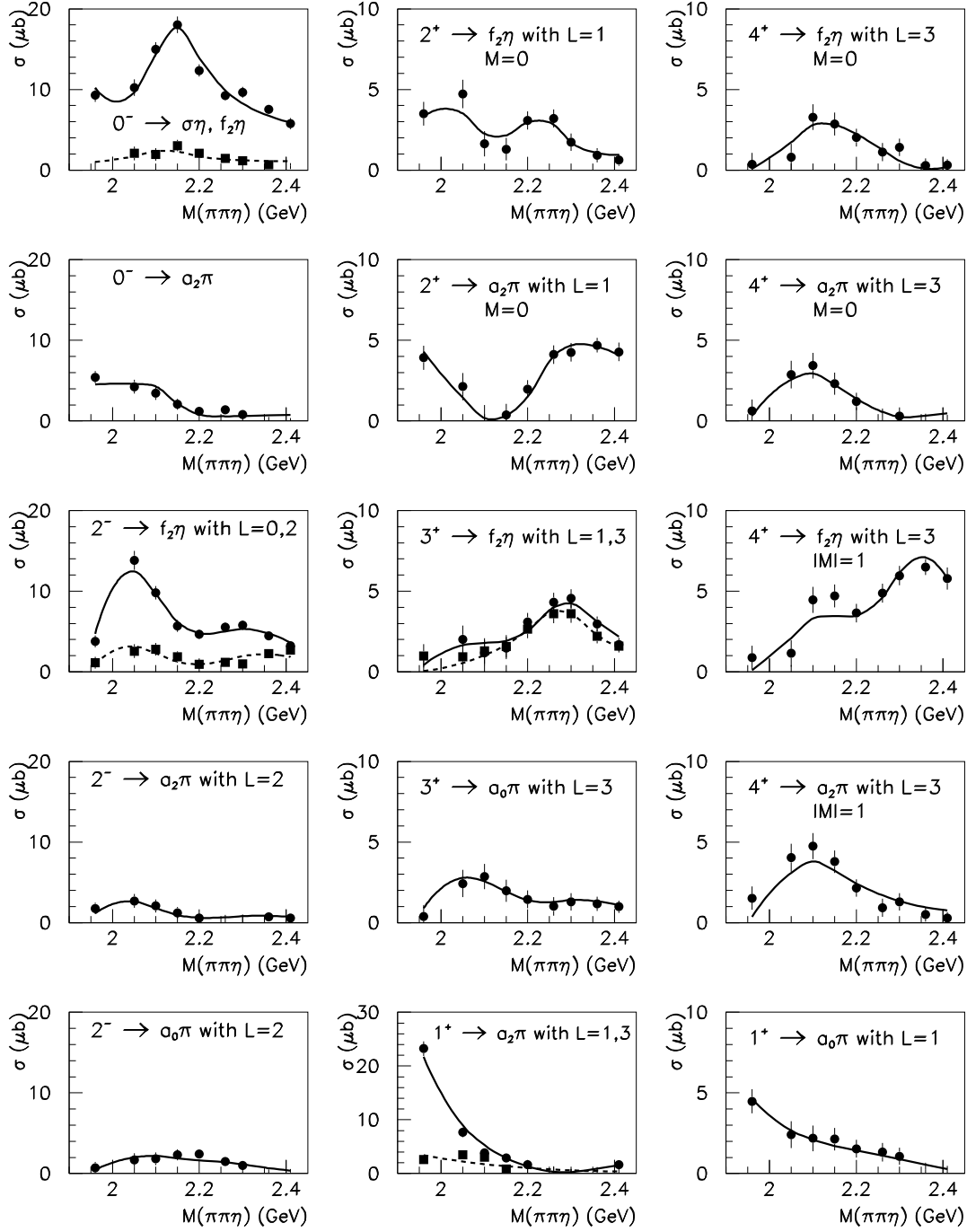


Figure 6. Cross sections for partial waves of significant contributions to  $\bar{p}p \rightarrow \pi^0\pi^0\eta$  with  $\eta \rightarrow \gamma\gamma$ . For diagrams with two components, the first label (full line) corresponds to the bigger component. The curves are the fit of Breit-Wigner amplitudes to the data points in the figure and the relative phases between components.

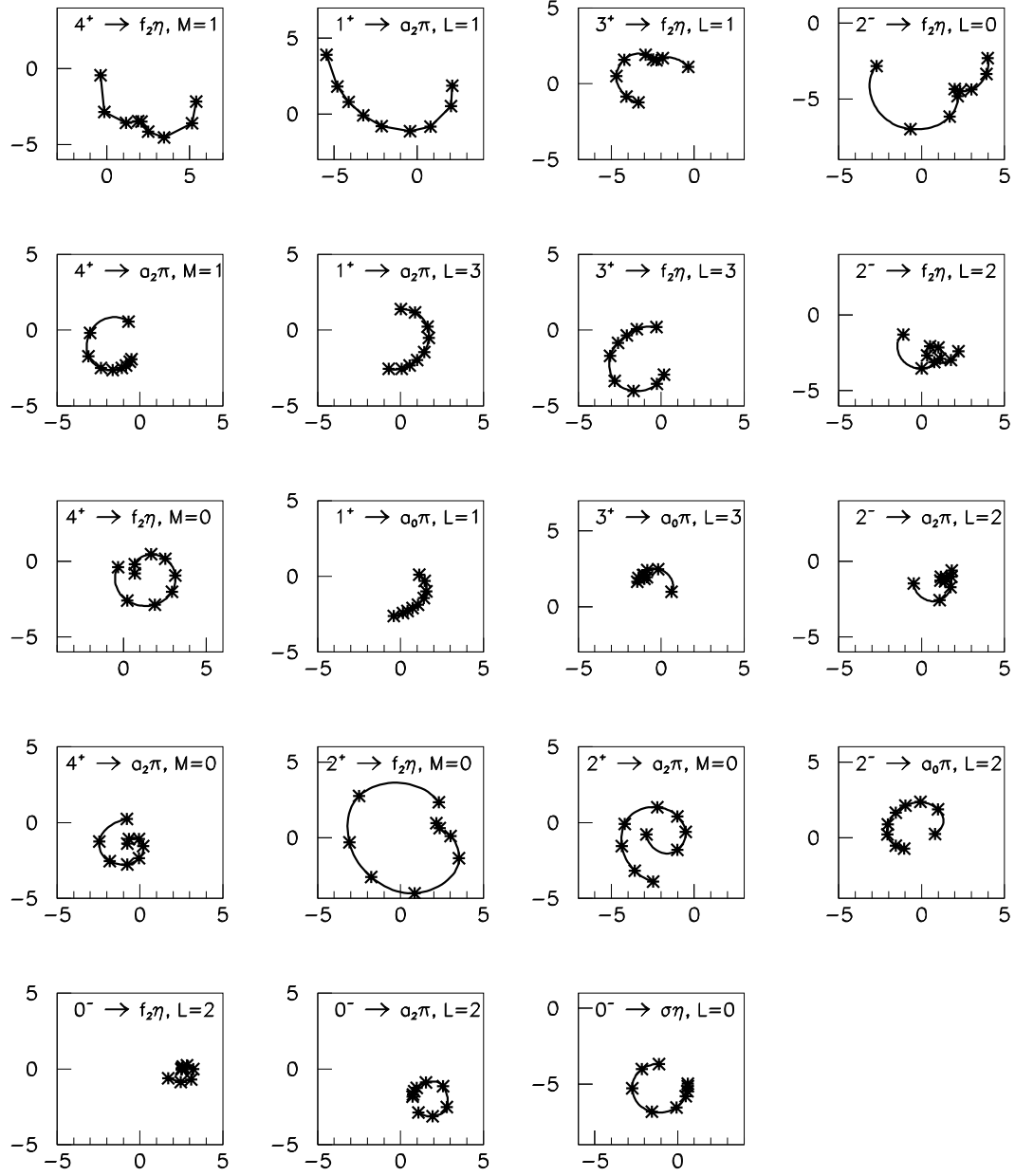


Figure 7. Argand plots corresponding to curves of Fig.6



Table 2

Summary of fitted masses, widths and branching ratios corrected for their unseen decay modes. The mass and width of  $f_4(2050)$  are fixed at PDG values, and the status of the  $0^-$  state at 2140 MeV is questionable, as discussed in the text. The  $f_1(1700)$  is beyond the accessible mass range. All states have  $I = 0$ ,  $G = +1$ .

$J^{PC}$	M(MeV)	$\Gamma(\text{MeV})$	$\frac{\Gamma_{\bar{p}p}\Gamma_{f_2\eta}}{\Gamma_{tot}^2}10^3$	$\frac{\Gamma_{\bar{p}p}\Gamma_{a_2\pi}}{\Gamma_{tot}^2}10^3$	$\frac{\Gamma_{\bar{p}p}\Gamma_{\sigma\eta}}{\Gamma_{tot}^2}10^3$	$\frac{\Gamma_{\bar{p}p}\Gamma_{a_0\pi}}{\Gamma_{tot}^2}10^3$
$4^{++}$	2044	208	$0.54 \pm 0.14$	$5.1 \pm 0.8$	-	-
$4^{++}$	$2320 \pm 30$	$220 \pm 30$	$1.3 \pm 0.4$	$1.0 \pm 1.0$	-	-
$3^{++}$	$2000 \pm 40$	$250 \pm 40$	$0.12 \pm 0.08$	$0.6 \pm 0.6$		$0.23 \pm 0.11$
$3^{++}$	$2280 \pm 30$	$210 \pm 30$	$1.7 \pm 0.4$	$4.5 \pm 2.6$		$0.23 \pm 0.19$
$2^{++}$	$2020 \pm 50$	$200 \pm 70$	$2.1 \pm 0.4$	$4.3 \pm 1.2$	-	-
$2^{++}$	$2240 \pm 40$	$170 \pm 50$	$2.5 \pm 0.6$	$1.6 \pm 1.6$	-	-
$2^{++}$	$2370 \pm 50$	$320 \pm 50$	$0.88 \pm 0.64$	$16 \pm 5$	-	-
$1^{++}$	$\sim 1700$	$\sim 270$				
$1^{++}$	$2340 \pm 40$	$340 \pm 40$	$0.6 \pm 0.6$	$60 \pm 30$		$0.84 \pm 0.53$
$0^{-+}$	$2140 \pm 30$	$150 \pm 30$	$1.9 \pm 1.7$	$6.0 \pm 6.0$	$10 \pm 5$	
$2^{-+}$	$2040 \pm 40$	$190 \pm 40$	$3.0 \pm 0.3$	$5.0 \pm 2.1$		$0.4 \pm 0.2$
$2^{-+}$	$2300 \pm 40$	$270 \pm 40$	$2.8 \pm 0.7$	$2.0 \pm 2.0$		$0.5 \pm 0.5$

Using interfering sums of the Breit-Wigner amplitudes to fit the partial wave cross sections in Fig.6 as well as relative phases between different partial waves, we obtain the masses, widths and branching ratios shown in Table 2. The corresponding Argand plots for all partial waves are shown in Fig.7. Besides the obvious resonances mentioned in previous paragraphs, we need another  $1^{++}$  resonance at about 2340 MeV with width  $\sim 270$  MeV. Without it, we cannot describe the relative phase between  $1^{++}$  and  $4^{++}$  partial waves; also we would need the lower  $1^{++}$  resonance to be very narrow ( $< 50$  MeV) in order to explain the sharp increase in the  $1^{++}$  partial wave cross section at low mass. In our present fit with two  $1^{++}$  resonances, the  $f_1(2340)$  amplitude interferes destructively with the tail of the lower  $1^{++}$  resonance and causes the sharply decreasing cross section with a broad dip around 2340 MeV. The phase motion caused by this  $f_1(2340)$  can be seen clearly in the Argand plot for the  $1^{++} \rightarrow a_2\pi$  partial wave in Fig.7.

In Table 2, the branching ratios are calculated at the resonance masses and are corrected for their unseen decay modes, except for  $a_0(980)$  where  $\Gamma_{a_0\pi} = \Gamma_{a_0\pi \rightarrow \eta\pi\pi}$ .

Among these resonances, the  $\eta(2140)$  and  $f_2(2240)$  look special. Both have relative narrow decay width. The  $\eta(2140)$  decays dominantly into  $\eta\sigma$ ; the  $f_2(2240)$  has the largest  $f_2\eta/a_2\pi$  ratio. These properties suggest that they may have larger mixing of glue components than other resonances.

#### 4. SUMMARY AND OUTLOOK

In summary, from a full amplitude analysis of  $\bar{p}p \rightarrow \pi^0\pi^0\eta$  in-flight, we have observed a new decay mode  $\eta\pi\pi$  for three established resonances  $f_4(2050)$ ,  $f_2(2010)$  and  $f_2(2340)$ .

In addition, we have observed 8 new or poorly established resonances in the energy range from 1960 to 2410 MeV, i.e.,  $f_4(2320)$ ,  $f_3(2000)$ ,  $f_3(2280)$ ,  $f_2(2240)$ ,  $f_1(2340)$ ,  $\eta(2140)$ ,  $\eta_2(2040)$  and  $\eta_2(2300)$ . Among them, the  $0^{-+}$   $\eta(2150)$  has very large decay branching ratio to  $\eta\sigma$ ;  $2^{++}$   $f_2(2230)$  has the largest  $f_2\eta/a_2\pi$  ratio; both have relative narrow total decay width. These properties suggest that they may have larger glueball components.

For a further study of the  $\eta(2140)$  and  $f_2(2240)$ , we are going to reconstruct  $\pi^0\pi^0\eta'$  channel from  $10\gamma$  events, where we expect less contamination from other channels. The main purpose here is to scan the  $f_2\eta'$  and  $\sigma\eta'$  modes which are also expected to be favourable decay modes of glueballs.

We are also going to scan  $f_2\pi^0$  from  $\pi^0\pi^0\pi^0$  final state to study isovector  $q\bar{q}$  states and scan  $f_2\omega$  from  $\pi^0\pi^0\omega$  final state to study isoscalar  $q\bar{q}$  states. Both  $\pi^0\pi^0\pi^0$  and  $\pi^0\pi^0\omega$  channels have enough statistics for a full amplitude partial wave analysis and have  $f_2$  band as their most obvious contribution in their Dalitz plots.

From these analyses of three-body annihilation in-flight, combined with information from two-body annihilations, we hope to establish the  $2.0 \sim 2.4\text{GeV}/c^2$  meson spectroscopy which is crucial for identifying glueballs and understanding quark confinement.

**Acknowledgement:** I thank the organizers of the LEAP98 conference for the invitation to give the talk in such a nice place, Sardinia. I am very grateful to D.V.Bugg and A.V.Sarantsev for the fruitful collaboration on data analysis, and to Crystal Barrel Collaboration for producing the beautiful data.

## REFERENCES

1. C.Michael, these proceedings; G.Bali et al. (UKQCD), Phys. Lett. **B307** (1993) 378; H.Chen, J.Sexton, A.Vaccarino and D.Weingarten, Nucl. Phys. B (Proc. Suppl.) 34 (1994) 357; X.Q.Luo et al., Nucl. Phys. **B53** (Proc. Suppl.) (1997) 243.
2. V.V.Anisovich et al., Phys.Lett. **B 323** (1994) 233; Phys. Rev. **D50** (1994) 1972; C.Amsler et al., Phys. Lett. **B355** (1995) 425.
3. K.Braune, these proceedings and references therein.
4. D.V.Bugg, these proceedings; A.Abele et al.,  $\pi^0\eta\eta$  papers, to be published.
5. V.A.Novikov, M.A.Shifman, A.I.Vainshtein and V.I.Zakhnov, Nucl. Phys. B 191 (1981) 301.
6. J.Y.Cui, J.M.Wu and H.Y.Jin, Phys. Lett. B424 (1998) 381.
7. Particle Data Group, C. Caso et al., Euro. Phys. J. C3 (1998) 1.
8. D.V.Bugg et al., Phys. Lett. B353 (1995) 378.
9. A.Abele et al.,  $\pi^0\pi^0\eta$  papers, to be published.
10. A.Hasan and D.V.Bugg, Phys. Lett. B334 (1994) 215.
11. A.Bertin et al., Phys. Rev. D57 (1998) 55.
12. S.U.Chung, Phys. Rev. D48 (1993) 1225; D57 (1998) 431.
13. V.Filippinni, A.Fontana and A.Rorondi, Phys. Rev. D51
14. D.V.Bugg, A.V.Sarantsev and B.S.Zou, Nucl. Phys. **B471** (1996) 59.
15. D. Ryabchikov, *Hadron Spectroscopy*, AIP Conf. Proc. (full reference to follow).
16. BES collaboration, J.Z.Bai et al., Phys. Rev. Lett. **76** (1996) 3502.
17. D.V.Bugg and B.S.Zou, Phys. Lett. B396 (1997) 295.